Robotica: (2019) volume 37, pp. 1332–1345. © Cambridge University Press 2019
doi:10.1017/S0263574718001546

Analysis and Evaluation on Unloading Ratio of Zero-g Simulation System Based on Torques of Space Manipulator

Sihui Tian†, Xiaoqiang Tang†‡* and Yuqi Li†

† *State Key Laboratory of Tribology, Department of Mechanical Engineering, Tsinghua University, Beijing, China. E-mails: tsh14@mails.tsinghua.edu.cn; liyuqi_ustb@163.com*
‡ *Beijing Key Lab of Precision/Ultra-Precision Manufacturing Equipments and Control, Tsinghua University, Beijing, China*

(Accepted December 22, 2018. First published online: January 31, 2019)

SUMMARY
In this paper, a dynamic model of a seven-joints manipulator operated in a zero-g simulation system is established. The errors of the friction, the suspension force, and the flexible deformation of arms are considered. Furthermore, the unloading ratio, which can evaluate the performance of the simulation system, is presented. It can reflect the level of similarity between the system and the space environment directly and effectively. The results of experimental and theoretical analyses verify the correctness of the model. It helps us to get the joint torques when the actual space manipulator without the torque sensor operates in this system and guarantees the safety of the experiments.

KEYWORDS: Unloading ratio; Zero-g simulation; Space manipulator; Joint torque.

1. Introduction

As one of the most important equipment on the space station, the space manipulator can achieve a variety of on-orbit servicing missions such as mounting the components, repairing the equipment, assisting the astronauts in space walking and docking, and refueling for spacecrafts.[1–3] To guarantee the safety and reliability on orbit, the space manipulator should be analyzed and should pass all the verification tests in a zero-g simulation system on ground.[4–6]

The simulation system should simulate the space environment and allow movements of the manipulator in a safety condition. Therefore, we present an index "the unloading ratio" to evaluate the performance of the system. Scholars used some indexes to guarantee the safety and reliability of the system . Sato[7] presented and compared two methods, which are "Suspension through center of mass" and "Suspension through joints," to achieve the constant tension. Junshan et al.[8] studied the angular deviation of the suspension system to detect the performance of the simulation system. Liu[9] established the relationship between the subsidiary stress and tension force errors as the evaluation index of the simulation system. While in the former studies, they focused more on the achievement of the experiments, and the specific data were always ignored. A great difference may exist between the manipulator operating in the ground experiment and on orbit. In this study, we use the joint torques as the parameters to calculate the unloading ratio. It can be used to predict the operating condition of the manipulator on orbit as well.

To obtain the joint torques, a simulated manipulator, which is installed with the torque sensors and has the much lower cost, was designed. It replaces the actual space manipulator for the initial tests, which can consummate the simulation system and guarantee the safety in the experiments of the space manipulator. The theoretical model of the joint torques needs to be established. In general, it is

* Corresponding author. E-mail: tang-xq@mail.tsinghua.edu.cn

a problem in robot dynamics. The dynamical equations can be formulated via several methods. Tian et al.[10] established the dynamical model of a manipulator by using the Newton–Euler laws. They considered the mass deviation and inertia based on constant mass. Korayem et al.[11] formulated the dynamic load for a flexible link manipulator using the finite element method. But it only suits for the robot which is not complicated. Zhang et al.[12] presented a dynamic model of a space flexible probe-cone docking system based on the Kane method. This method makes the modeling process much easier than that of the Lagrange method. Liu and Huang[13] established the dynamics of flexible-joint robot manipulators, which make contributions to the further work of the manipulator control with parameter uncertainties and external disturbances. In this study, to simplify the calculation and guarantee the accuracy of the theoretical model in the meantime, we use the method that combines the finite element method with the Newton–Euler laws.

While, there are still some errors that cannot be ignored in the simulation system. Ijar et al.[14] indicated that the simulation system was sensitive to any reaction force. The forces will change the motion of the manipulator and it will cause the additional torques. Morel et al.[15] presented the joint friction was a major problem in the accurate robot position control. They used the torque sensor mounted under the manipulator as the feedback to compensate for the joint friction. Brown and Dolan[16] calculated the angle-to-torque transfer functions when the string had a deflection angle with the vertical direction. López-Martínez et al.[17] presented a detailed multibody model of a robot arm to control the force and the position of the end, which is more accurate and reliable compared to the previous methods. Simoni et al.[18] considered the friction of industrial robots effects of the temperature and verified the effectiveness of the theoretical model. In our system, the errors are various and complicated. While, the core of this paper is to build a frame of the dynamic model for the simulation system. Therefore, we only consider the deviation of suspension forces, frictions, and the elastic deformation of arms in a simplified way.

In this paper, a dynamic model with error corrections of a seven-joints manipulator operated in a zero-g simulation system is established. A new index "the unloading ratio" is presented to evaluate the experiment results and the accuracy of the model. Furthermore it can reflect the level of similarity between the system and the space environment directly. This work can help us to calculate the joint torques when the actual space manipulator without the torque sensor operates. The paper is organized as follows. In Section 2, the zero-g simulation system and the manipulator are introduced. The definition of unloading ratio is presented in Section 3. The theoretical model and the errors are analyzed and established in Section 4. In Section 5, the simulation results are considered and the errors are derived. The comparison between the theoretical and the experimental results is presented in Section 6. Conclusions are drawn in Section 7.

2. Introduction of Zero-g Simulation System with Space Manipulator

The structure of the zero-g simulation system is shown in Fig. 1. It contains a suspension system and a manipulator. The suspension system can be divided into two distinct parts: a constant tension force system and a follow-up system. The tension force system affords vertical force and adjusts the length of the sling by using a constant torque motor and a specific structure, which can balance the gravity . The follow-up system can move in two directions, which guarantees the tension force vertically whatever the attitude of the manipulator is. The manipulator is a seven-rotary degree of freedom (DOF) serial robot, which consists of seven sets of interchangeable revolute joints, two arms, two end effectors, and one central controller. A torque sensor is installed in each joint to avoid exceeding the limit. One of the end effectors is fixed on the support frame, while another one can reach the target. Except the arms, the other components are connected with the sub-slings by the suspension parts. Because the relative motion of the barycenter of two adjacent components is tiny, when the manipulator operates, two adjacent sub-slings can be combined into a top-sling by a rod structure. It simplifies the simulation system. Therefore, this system has 10 sub-slings and 5 top-slings. Each top-sling connects with one suspension system directly.

To describe the geometry of the manipulator, starting from the basic, we number the components sequentially from C1 to C10, wherein C1 and C10 are the end effectors, C6 is the central controller, and the others are joints. A Cartesian coordinate system is established and the D-H rotation matrices[19] can be obtained:

$$^{i}\mathbf{R}_{i+1} = \mathbf{R}_z(\theta_{zi})\mathbf{R}_y(\theta_{yi})\mathbf{R}_x(\theta_{xi}), \tag{1}$$

https://doi.org/10.1017/S0263574718001546 Published online by Cambridge University Press

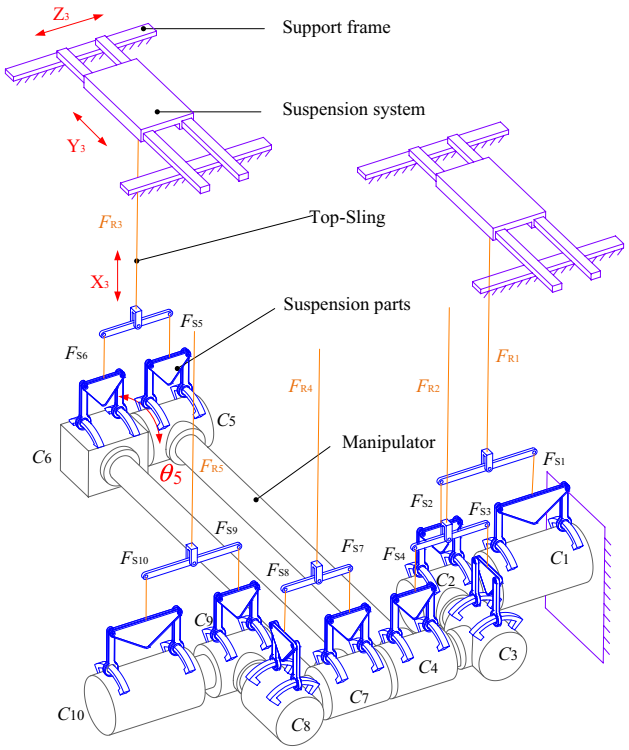

Fig. 1. Structure of the zero-g simulation system.

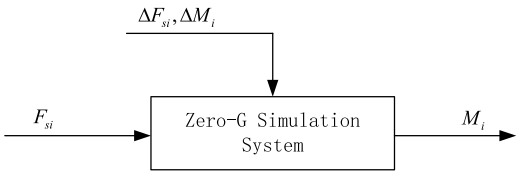

Fig. 2. Inputs and outputs chart of the simulation system.

where the matrices ${}^{i}\mathbf{R}_{i+1}$ means from the ith joint to the $i+1$th joint. θ_{zi}, θ_{yi}, and θ_{xi} are the roll, pitch yaw angles about OX, OY, OZ axis.

Inputs and outputs chart of this system is illustrated in Fig. 2. The mass and structure of the manipulator are the intrinsic parameters, the suspension forces $\mathbf{F}_{si}(i = 1, \ldots, 10)$ and the angle of joints $\theta_i(i = 1, \ldots, 10)$ are the inputs; the joint torques $\mathbf{M}_i(i = 1, \ldots, 10)$ are the outputs; meanwhile, the errors such as the tension errors $\Delta\mathbf{F}_{si}(i = 1, \ldots, 10)$, frictions and deformations, which are represented as $\Delta\mathbf{M}_i$, cannot be ignored.

The force balance equation can be written as

$$\begin{cases} \sum \mathbf{F}_{si} + \sum \mathbf{G}_i + \sum \Delta\mathbf{F}_{si} = f(\dot{v}(\theta_i)) \\ \sum \mathbf{M}_i + \sum \Delta\mathbf{M}_i + \sum \mathbf{F}_{si} \cdot \mathbf{l}_{si} + \sum \mathbf{G}_i \cdot \mathbf{l}_{Gi} + \sum \Delta\mathbf{F}_{si} \cdot \mathbf{l}_{si} = f(\dot{\omega}(\theta_i), \omega(\theta_i)) \end{cases}, \tag{2}$$

where $f(\dot{v}(\theta_i))$ and $f(\dot{\omega}(\theta_i), \omega(\theta_i))$ are the inertia force and inertia torque, which are the function of θ_i. $\mathbf{l}_{Si}$ and $\mathbf{l}_{Gi}$ are the coordinate of the suspension point and the barycenter of the joint. $\mathbf{G}_i$ is the gravity of the component.

3. Definition of Unloading Ratio

As the direct output of the system, the joint torques can reflect whether the experiments simulate the zero-g environment successfully. While, this manipulator has seven joints, and the torques are changed all the time. Therefore, the unloading ratio, which is based on the joint torques, is presented. It is an index that evaluates the simulation system directly and effectively.

https://doi.org/10.1017/S0263574718001546 Published online by Cambridge University Press

Table I. Parameters used in dynamics.

Symbol	Parameter
$\mathbf{v}_i$	Linear velocity of point O_i
ω_i	Angular velocity of link i
$\dot{\mathbf{v}}_i$	Linear acceleration of point O_i
$\dot{\omega}_i$	Angular acceleration of link i
$\tilde{\dot{\mathbf{v}}}_i$	Linear acceleration of barycenter of link i
$\mathbf{e}_i$	Unit vector pointing along z_i-axis
$\mathbf{p}_{i,i+1}$	Position velocity of point O_{i+1} with respect to point O_i
$\mathbf{r}_i$	Position velocity of barycenter of link i with respect to point O_i
$\mathbf{f}_i$	Resulting force exerted on link i by link $i-1$ at point O_i
τ_i	Resulting torque exerted on link i by link $i-1$ at point O_i
$\mathbf{F}_i$	Inertia force exerted at barycenter of link i
$\mathbf{M}_i$	Inertia torque exerted at barycenter of link i

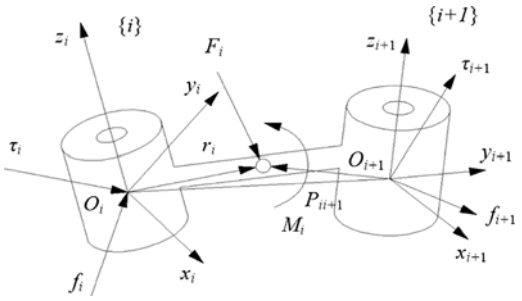

Fig. 3. Experimental and theoretical torques of joint.

In a particular sequence, the unloading ratio for single joint η_i is defined as

$$\eta_i = \begin{cases} 0 & M_{iz} \geq M_{lim} \\ 1 - \dfrac{\int |M_{iz}| dt}{M_{lim} t} & M_{iz} < M_{lim} \end{cases}. \tag{3}$$

where M_{lim} is the limit torque of the joints, M_{iz} is the joint about the z-axis. When the experimental torque is beyond the limit, the unloading ratio is 0, which means the condition cannot satisfy the requirements. The experiment must be stopped immediately. In space, the unloading ratio is near to 1 for the tiny joint torque.

Considering seven joints, the total unloading ratio η is defined as

$$\eta = 1 - \sqrt{\frac{\sum_{i=1}^{7} (1-\eta_i)^2}{7}}. \tag{4}$$

If the total unloading ratio is closer to 1, the simulation system is more similar to the zero-g environment.

4. Theoretical Modeling of Manipulator

4.1. Torque of joint

The link parameters are illustrated in Fig. 3. Two adjacent links are i and i+1, and the link reference coordinates are i and i+1. The following parameters are employed to establish the equations, presented in Table I. The subscript i means that the parameter expresses in the coordinate system of link i.

The recursion formula for the linear acceleration of the barycenter is computed as

$$\tilde{\dot{\mathbf{v}}}_{i+1} = \dot{\mathbf{v}}_{i+1} + \dot{\omega}_{i+1} \times \mathbf{r}_{i+1} + \omega_{i+1} \times (\omega_{i+1} \times \mathbf{r}_{i+1}). \tag{5}$$

https://doi.org/10.1017/S0263574718001546 Published online by Cambridge University Press

The recursion formula of the inertia force and inertia torque are obtained

$$\begin{aligned} \mathbf{F}_{i+1} &= m_{i+1}\tilde{\dot{\mathbf{v}}}_{i+1}, \\ \mathbf{M}_{i+1} &= \tilde{\mathbf{I}}_{c_{i+1}}\dot{\omega}_{i+1} + \omega_{i+1} \times \tilde{\mathbf{I}}_{c_{i+1}}\omega_{i+1}, \end{aligned} \tag{6}$$

where m_{i+1} is the mass of link $i+1$ and $\tilde{\mathbf{I}}_{c_{i+1}}$ is the inertial matrix in the barycentric coordinate system.

The backward expressions are

$$\begin{aligned} \mathbf{f}_i &= \mathbf{F}_i + {}^{i}_{i+1}\mathbf{R}\mathbf{f}_{i+1}, \\ \tau_i &= \mathbf{M}_i + {}^{i}_{i+1}\mathbf{R}\tau_{i+1} + \mathbf{r}_{i+1} \times \mathbf{F}_i + \mathbf{p}_{i,i+1} \times {}^{i}_{i+1}\mathbf{R}\mathbf{f}_{i+1}. \end{aligned} \tag{7}$$

When the manipulator operates in the active compensation suspension system, it is exerted by suspension forces and gravity. Ideally, the suspension forces can balance the gravity. However, there are some deviations in the values, directions, and point of application of the suspension force, which cause the inertia forces and the inertia torques at barycenter of each joint.

Assume the mass of link i is m_i and the suspension force is $\mathbf{F}_{s_i}$. The suspension force and the gravity of link i are transformed into the link i coordinate system as follows:

$$\begin{aligned} \mathbf{F}_{s_i}{}' &= {}^{i}_{0}\mathbf{R}\mathbf{F}_{s_i}, \\ \mathbf{G}_i{}' &= m_i\, {}^{i}_{0}\mathbf{R}\mathbf{g} = {}^{i}_{0}\mathbf{R}m_i\mathbf{g}. \end{aligned} \tag{8}$$

Because the torque about the z-axis is much larger than that about the other two axes, and the torque sensor is designed to collect the z-axis torque, we only consider the torque about the z-axis. By substituting Eq. (8) into Eq. (7), the backward force and torque expressions can be established:

$$\begin{aligned} \mathbf{f}_i &= F_i + {}^{i}_{i+1}\mathbf{R}\mathbf{f}_{i+1} + {}^{i}_{0}\mathbf{R}(\mathbf{F}_{s_i} - m_i\mathbf{g}), \\ \tau_{iz} &= (\mathbf{M}_i + {}^{i}_{i+1}\mathbf{R}\tau_{i+1} + \mathbf{r}_{i+1} \times (F_i + ({}^{i}_{0}\mathbf{R}(\mathbf{F}_{s_i} - m_i\mathbf{g})) + \mathbf{p}_{i,i+1} \times {}^{i}_{i+1}\mathbf{R}\mathbf{f}_{i+1}) \cdot \mathbf{e}_i. \end{aligned} \tag{9}$$

Considering the errors of suspension forces, frictions and deformation of arms, the joint torque about the z-axis is expressed as

$$M_{iz} = \tau(\mathbf{F}_{si} + \Delta\mathbf{F}_{si}) + M_{\text{rail}} + M_{\text{joint}} + M_{\text{arm}}, \tag{10}$$

where M_{rail}, M_{joint} and M_{arm} are the torques from the frictions of the sliding rails, the frictions of the joints and the deformation of arms. These expressions of errors will be derived in the following subsections.

4.2. Deviation of suspension force

The control chart of the whole system is shown in Fig. 4. When the manipulator motions, the cameras and tension sensors collect the attitude of the manipulator and the sling tensions, and then send the data to the simulation system. The system calculates and controls the length and position of the slings. The time difference will cause the inclination which is involved in this section. While the stiffness of slings is large, the stiffness characteristic of slings can be ignored. The errors of a sling are illustrated in Fig. 5.

Assuming the ideal length of top-sling i is L_{Ri}, the force in top-sling i is F_{Ri}, the forces in sub-sling are F_{S2i} and $F_{S(2i-1)}$, the deviation of force F_{Ri} is ΔF_{Ri} , the deviation of position is $(\Delta x_i, \Delta y_i, \Delta z_i)$, the real value of sling force is

$$F'_{Ri} = F_{Ri} + \Delta F_{Ri}, \tag{11}$$

and the real value of the sling length is

$$L'_{Ri} = \sqrt{(L_{Ri} + \Delta x_i)^2 + \Delta y_i^2 + \Delta z_i^2}. \tag{12}$$

According to the parameters of the rod in Fig. 5, the force balance equations are expressed as

https://doi.org/10.1017/S0263574718001546 Published online by Cambridge University Press

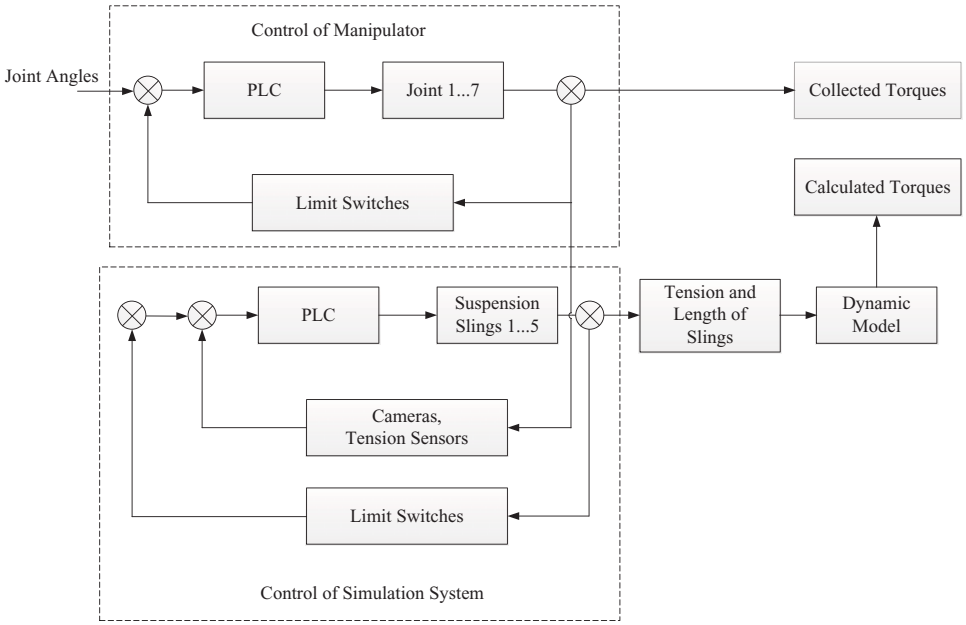

Fig. 4. Simplified control chart of whole system.

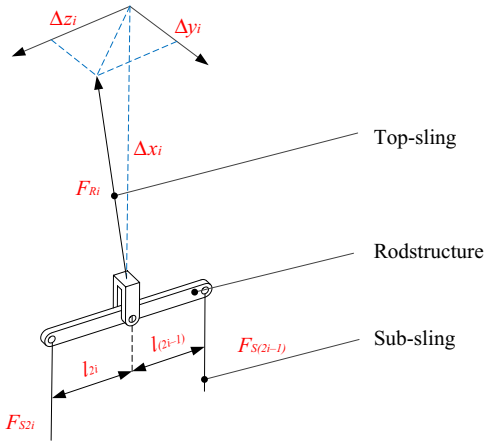

Fig. 5. Deviation parameters of sling.

$$\begin{cases} F'_{Ri} = F_{S2i} + F_{S(2i-1)} \\ \dfrac{F_{S(2i-1)}}{F_{S2i}} = \dfrac{l_{S2i}}{l_{S(2i-1)}} = p_{2i} \end{cases}, \tag{13}$$

where p_{2i} is the proportionality factor of the position of the sub-slings.

The value of sub-sling force depends on the sling force and the structure of the rod:

$$\begin{cases} F_{S(2i-1)} = \dfrac{p_{2i}}{1+p_{2i}} \cdot F'_{Ri} \\ F_{S2i} = \dfrac{1}{1+p_{2i}} \cdot F'_{Ri} \end{cases}. \tag{14}$$

Therefore, considering the errors, the suspension force is as follows:

$$\mathbf{F}'_{Ri} = \left(\frac{L_{Ri} + \Delta x_i}{L'_{Ri}}, \frac{\Delta y_i}{L'_{Ri}}, \frac{\Delta z_i}{L'_{Si}} \right)^T \cdot (F_{Ri} + \Delta F_{Ri}). \tag{15}$$

By substituting Eq. (15) in Eq. (14), the sub-sling force after correction are expressed as

https://doi.org/10.1017/S0263574718001546 Published online by Cambridge University Press

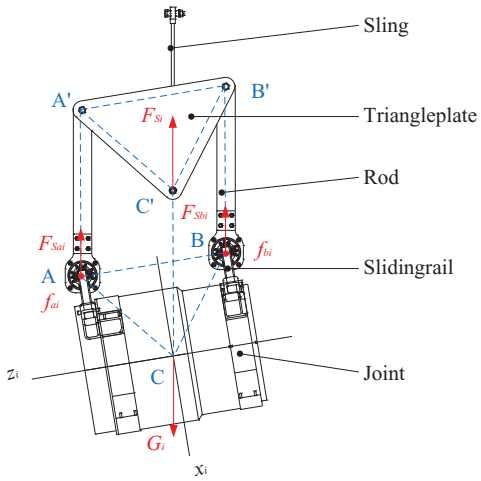

Fig. 6. Model of a suspension unit.

$$\begin{cases} \mathbf{F}_{S(2i-1)} = \dfrac{p_{2i}}{1+p_{2i}} \cdot \left(\dfrac{L_{Ri}+\Delta x_i}{L'_{Ri}}, \dfrac{\Delta y_i}{L'_{Ri}}, \dfrac{\Delta z_i}{L'_{Si}} \right)^T \cdot (F_{Ri}+\Delta F_{Ri}) \\ \mathbf{F}_{S2i} = \dfrac{1}{1+p_{2i}} \cdot \left(\dfrac{L_{Ri}+\Delta x_i}{L'_{Ri}}, \dfrac{\Delta y_i}{L'_{Ri}}, \dfrac{\Delta z_i}{L'_{Si}} \right)^T \cdot (F_{Ri}+\Delta F_{Ri})' \end{cases} . \tag{16}$$

4.3. Errors of friction

The friction error and parameter identification is complex. To calculate the data efficiently, we consider the friction as a kinematic problem. The source of the frictions in this simulation system is divided into two parts: joint frictions and the frictions caused by the motion between the sliding rail and the rod. Because of the bearing and the good lubrication, the joint frictions are little. The frictions between the sliding rail and the rod are the sliding frictions. During the startup motion of the manipulator, the frictions are created suddenly, which have great influence on the joint torques. The torque of joint i considering the frictions can be expressed as

$$M'_i = \tau_i + \left(\sum M_{\text{joint}} \right)_i + \left(\sum M_{\text{rail}} \right)_i , \tag{17}$$

where M_{joint} is the additional torque caused by the joint torque, M_{rail} is the additional torque caused by the rail.

Figure 6 shows a suspension unit, which consists of a joint and its suspension parts. Two sliding rails are fixed on the joint. The rod hinged with the triangle plate on the point A and B can slide on the sliding rail. The connection points are A and B. The sling connected to the point C at one end suspends the whole unit. Point C is the barycenter of the joint. According to the similarly suspension mechanism,[9] we can change the parameters of the triangle plate and rods to obtain $\triangle ABC \cong \triangle A'B'C'$. It can achieve the extension line of the suspension force through the barycenter whatever the attitude of the joint.

The gravity of the triangle plate and rods is G_{Ti}, the gravity of the joint is G_i, the suspension force is F_{Si}, and the support forces and frictions related to two rods are F_{Sai}, F_{Sbi}, f_{ai}, f_{bi}. The force balance equations are as follows:

$$\begin{cases} F_{Sai} + F_{Sbi} = F_{Si} + G_{Ti} = -G_i \\ f_{ai} = \mu F_{Sai} \\ f_{bi} = \mu F_{Sbi} \end{cases} , \tag{18}$$

${}^i\mathbf{h}_{ai}$ and ${}^i\mathbf{h}_{bi}$ are the positions of the connection points A and B in the coordinate system of joint i. They are the function of joint angle θ_i:

$$\begin{cases} {}^i\mathbf{h}_{ai} = Rot(z, \theta_i) \cdot \mathbf{h}_{ai} \\ {}^i\mathbf{h}_{bi} = Rot(z, \theta_i) \cdot \mathbf{h}_{bi} \end{cases} , \tag{19}$$

https://doi.org/10.1017/S0263574718001546 Published online by Cambridge University Press

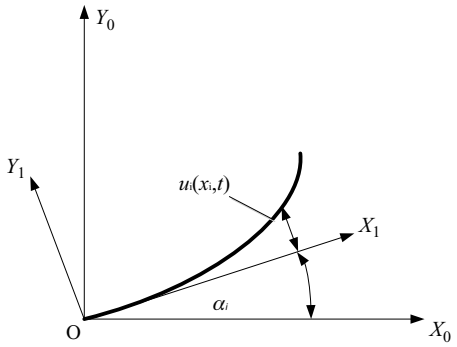

Fig. 7. Parameters and coordinate system of arm.

where $Rot(z,\theta_i) = \begin{pmatrix} \cos\theta_i & -\sin\theta_i & 0 \\ \sin\theta_i & \cos\theta_i & 0 \\ 0 & 0 & 1 \end{pmatrix}$ is the rotation matrix about the z-axis. Vectors $\mathbf{h}_{ai}$ and $\mathbf{h}_{bi}$ are the positions when the angle is zero, which are the constants about the structure of the joint.

The additional torque caused by the rail frictions to the joint i is computed as

$$ {}^{i}M_{\text{rail}i} = \begin{cases} ({}^{i}\mathbf{h}_{ai} \times \mathbf{f}_{ai} + {}^{i}\mathbf{h}_{bi} \times \mathbf{f}_{bi}) \cdot \mathbf{e}_i & \dot{\theta}_i \neq 0 \\ 0 & \dot{\theta}_i = 0 \end{cases}. \tag{20} $$

The points of friction in the coordinate system of the former joint k are expressed as

$$ \begin{aligned} \begin{pmatrix} {}^{k}\mathbf{h}_{ai} \\ 1 \end{pmatrix} &= {}^{k}\mathbf{T}_i \cdot \begin{pmatrix} \mathbf{h}_{ai} \\ 1 \end{pmatrix}, \\ \begin{pmatrix} {}^{k}\mathbf{h}_{bi} \\ 1 \end{pmatrix} &= {}^{k}\mathbf{T}_i \cdot \begin{pmatrix} \mathbf{h}_{bi} \\ 1 \end{pmatrix}, \end{aligned} \tag{21} $$

where ${}^{k}\mathbf{T}_i$ is the transformation matrix from k to i.

The additional torque caused by the rail frictions to the joint k is computed as

$$ {}^{k}M_{\text{rail}i} = \begin{cases} ({}^{k}\mathbf{h}_{ai} \times \mathbf{f}_{ai} + {}^{k}\mathbf{h}_{bi} \times \mathbf{f}_{bi}) \cdot \mathbf{e}_i & \dot{\theta}_i \neq 0 \\ 0 & \dot{\theta}_i = 0 \end{cases}. \tag{22} $$

Therefore, the additional torques of joint i include the friction torques from itself and the latter joints; it means

$$ \left(\sum M_{\text{rail}} \right)_i = \sum_{m=i}^{10} {}^{i}M_{\text{rail}\,m}. \tag{23} $$

The derivation of the additional torques caused by the joint frictions is similar. Hence, the joint torque considering the frictions is expressed as follows:

$$ M_i' = \tau_i + \sum_{m=i}^{10} {}^{i}M_{\text{joint}\,m} + \sum_{m=i}^{10} {}^{i}M_{\text{rail}\,m}. \tag{24} $$

4.4. Elastic deformation of arms

In this simulation system, the arm is suspended by both sides of the joint. For its high ratio of length to diameter, the stiffness is poor. It will cause the deformation and have effect on the joint torques. Figure 7 shows the parameters and the coordinate system of the arm.

To avoid a massive computational procedure, we consider the arm move in a two-dimensional plane. The global coordinate system is {global}. The coordinate system of the arm is $\{O - X_1Y_1\}$, in which the tangential direction of the arm is x-axis, α_i is the angle between X_1 and X_0:

$$ \mathbf{P}_i = (\mathbf{x}_i \cos\alpha_i - \mathbf{u}_i \sin\alpha_i)\mathbf{X}_0 + (\mathbf{x}_i \sin\alpha_i + \mathbf{u}_i \cos\alpha_i)\mathbf{Y}_0, \tag{25} $$

https://doi.org/10.1017/S0263574718001546 Published online by Cambridge University Press

Table II. Parameters of the manipulator.

	Joint	**Arm**	**End effector**	**Controller**
Mass/kg	67.7	25.5	87.3	37.7
Barycenter/mm	(−4.4,1.2,30)	(0,0,2200)	(−400,−13,−6.8)	(13.4,6.1,39.9)

where $\mathbf{u}_i(x_i, t)$ is a tiny deformation caused by elastic deformation. According to the assumed mode method[20], it can be expressed as

$$\mathbf{u}_i(x_i, t) = \mathbf{f}_i \mathbf{q}_i = \sum_{j=1}^{n} \varphi_{ij}(x_i) q_{ij}(t), \tag{26}$$

where $\mathbf{f}_i = [\varphi_{i1}, \ldots, \varphi_{in}]$ is the modal matrix, $\mathbf{q}_i = [q_{i1}, \ldots, q_{in}]^T$ is the Modal Coordinates. n means the number of the Modal Coordinates. The larger we choose, the more accurate the results are. Correspondingly, it will increase the computation.

The kinetic energy T_i and potential energy V_i can be computed as

$$\begin{aligned} T_i &= \frac{1}{2} J_i \dot{\alpha}_i^2 + \frac{1}{2} \rho_i A_i \int_0^L \dot{\mathbf{P}}_i^T \dot{\mathbf{P}}_i \mathrm{d}x_i \\ V_i &= \frac{1}{2} \int_0^L E_i I_i \left(\frac{\partial^2 u_i}{\partial x_i^2} \right)^2 \mathrm{d}x_i + m\mathbf{g} \cdot [0\ 1]\mathbf{P}_i \end{aligned}, \tag{27}$$

where J_i is the inertia moment, I_i is the inertia matrix, ρ_i is the material density, A_i is the cross-sectional of the arm and E_i is the modulus of elasticity.

By applying Lagrange equation[21]

$$\frac{\mathrm{d}}{\mathrm{d}t} \left(\frac{\partial T_i}{\partial \dot{q}_i} \right) - \frac{\partial T_i}{\partial q_i} + \frac{\partial V_i}{\partial q_i} = Q_i, \tag{28}$$

and making algebraic manipulations, the dynamic equations can be written in the following form:

$$\mathbf{M}(q_i)\ddot{q}_i + \mathbf{C}(q_i, \dot{q}_i)\dot{q}_i + \mathbf{K}_i q_i = \tau_i, \tag{29}$$

where $M(q_i)$ is the mass matrix, $C(q_i, \dot{q}_i)$ is the damping matrix and K_i is the stiffness matrix.

5. Analysis Result

Table II lists the parameters of the manipulator. According to the requirement of experiment, the initial attitude of the manipulator is that the joint 2 is 43°, the joint 6 is −43° and the others are 0°. When the position deviation of top-sling 1 (Δx_1, Δy_1, Δz_1) is changed by x-axis and y-axis, the joint torques are changed as well, shown in Fig. 8. It shows that the deviations have a great effect on the joint torques. 0.5 m deviation can make the torque change dozens or even hundreds units of $N \cdot m$. Joints 1, 3, 4 and 5 are sensitive to the changes on y-axis. While, joints 2 and 6 are sensitive to the changes on x-axis.

When only the value of suspension tensions changes, the joint torques are illustrated in Fig. 9. The torque gradients of joints 2, 3 and 4 are great, which means these joint torques are sensitive to the tension deviations.

When only the friction errors are considered, we calculate the torques as follows. Assuming the operation time sequence of the joint 1 is: (1) stops 30 s; (2) rotates clockwise through an angle 30° at a speed of $0.1°/s$; (3) rotates counterclockwise through an angle −30° at a speed of −0.1°/s. Substitute the parameters in Eq. 10 and illustrate the joint torques with the friction errors; Fig. 10 is obtained. The start or the direction change of the rotation will cause an abrupt change for the torques of joints 1, 3, 4 and 5, which is caused by the frictions. While, the abrupt change of joints 2 and 5 is little, because their z-axes are perpendicular to the plane of the triangle plate of joint 1, the cross product of position vector and friction approaches to 0.

Consider all the errors in the meantime. When joints 1–6 sequentially rotate as the operation time sequence mentioned before, the torques of seven joints are showed in Fig. 11. Because of the errors of suspension tensions and the flexible deformation of the arms, the curves are not as smooth as the

https://doi.org/10.1017/S0263574718001546 Published online by Cambridge University Press

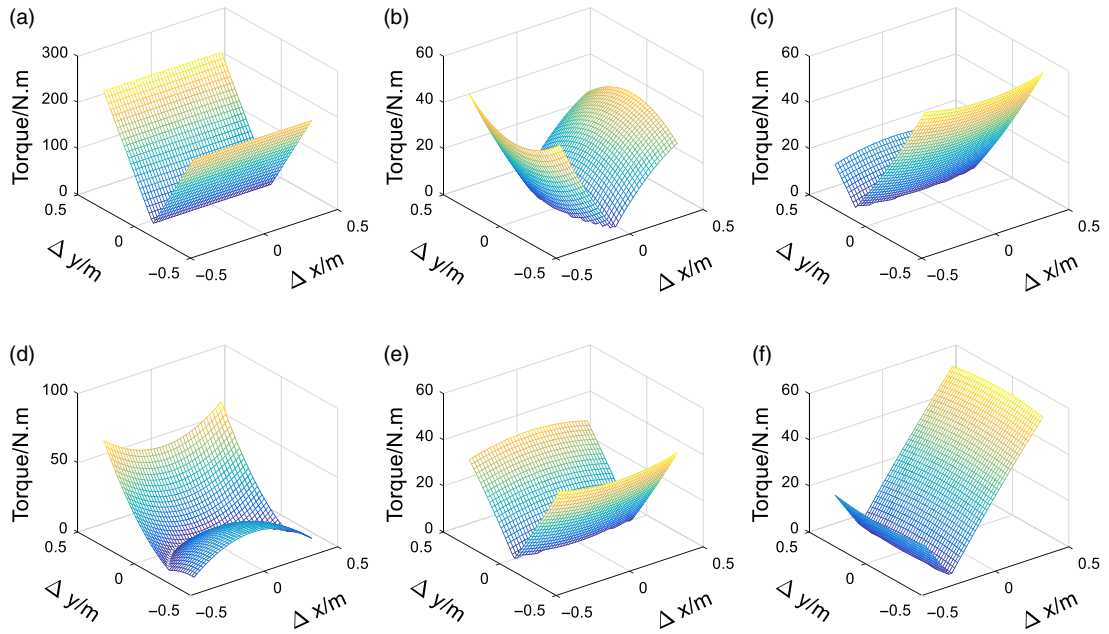

Fig. 8. Joint torques affected by position deviation of sling 1. (a) Torque of joint 1; (b) torque of joint 2; (c) torque of joint 3; (d) torque of joint 4; (e) torque of joint 5; and (f) torque of joint 6.

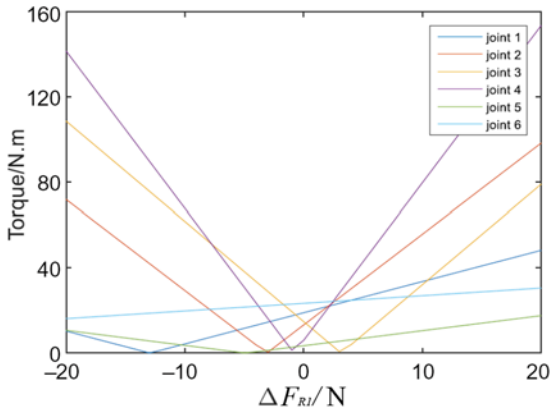

Fig. 9. Joint torques affected by tension deviation of slings.

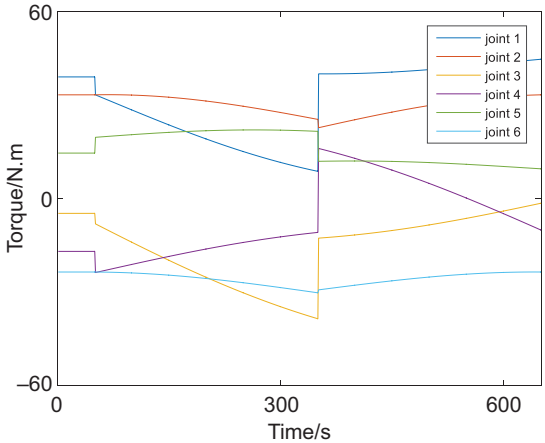

Fig. 10. Joint torques affected by friction.

https://doi.org/10.1017/S0263574718001546 Published online by Cambridge University Press

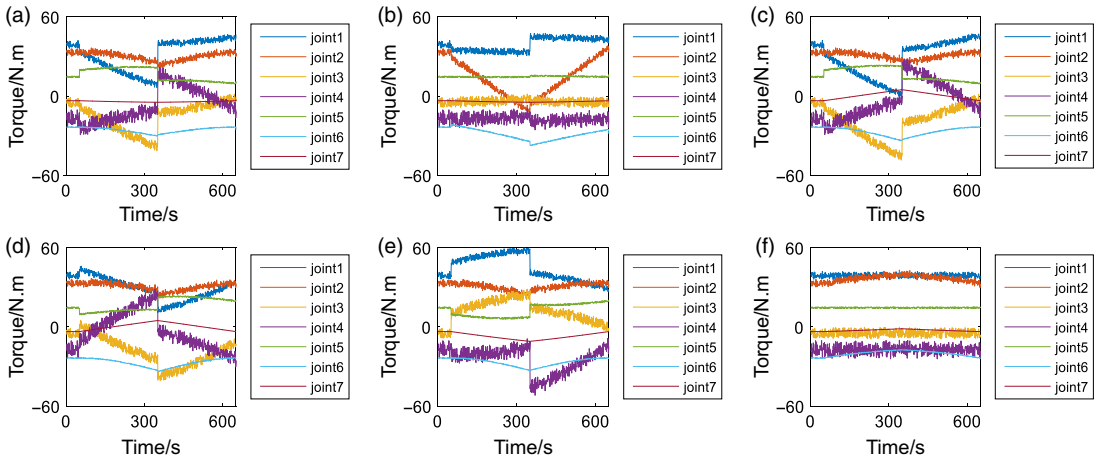

Fig. 11. Torque of each joint when joint 1 rotates. (a) Joint 1 rotates; (b) Joint 2 rotates; (c) Joint 3 rotates; (d) Joint 4 rotates; (e) Joint 5 rotates; and (f) Joint 6 rotates.

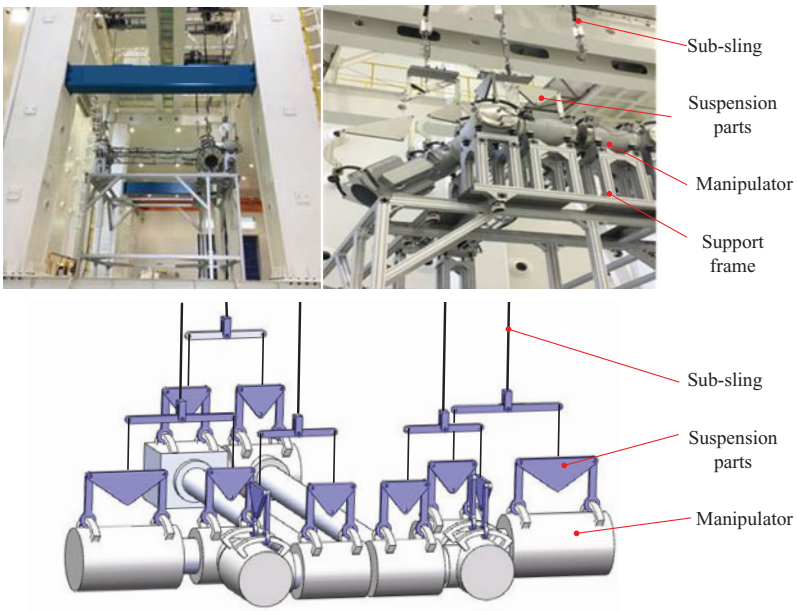

Fig. 12. Experiment field of the zero-g simulation system.

ideal ones. The torques of joints near the basic fluctuate obviously. When joints 1, 3, 4 or 5 rotate, the torques change suddenly as the start or the direction change of the joint operation; when the joint 2 rotates, the torques of joint 1 and 2 change obviously; the rotation of joint 6 has little effects on all torques.

6. Experiments and Results

6.1. Simulation system and motion of manipulator

Figure 12 is the photograph of the zero-g simulation system. Because this is the verification stage of the simulation system, the simulated manipulator replaces the actual space manipulator for the initial experiments. When the manipulator operates, one of the end effectors is fixed on the support frame, to simulate the space manipulator fixed on the astrovehicle. The other components will separate from the support frame. The suspension system affords the vertical constant force to balance the gravity. The torque sensors can collect the torque of each joint. The data can be used to evaluate the capability of the simulation system and monitor the safety of the manipulator.

https://doi.org/10.1017/S0263574718001546 Published online by Cambridge University Press

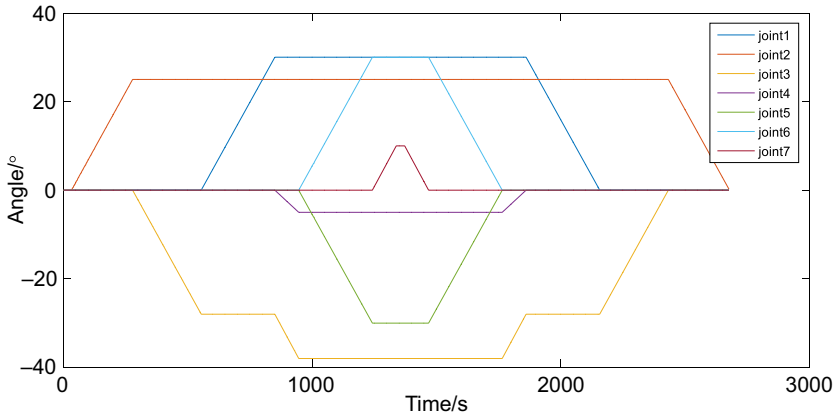

Fig. 13. Time sequences of joint rotations.

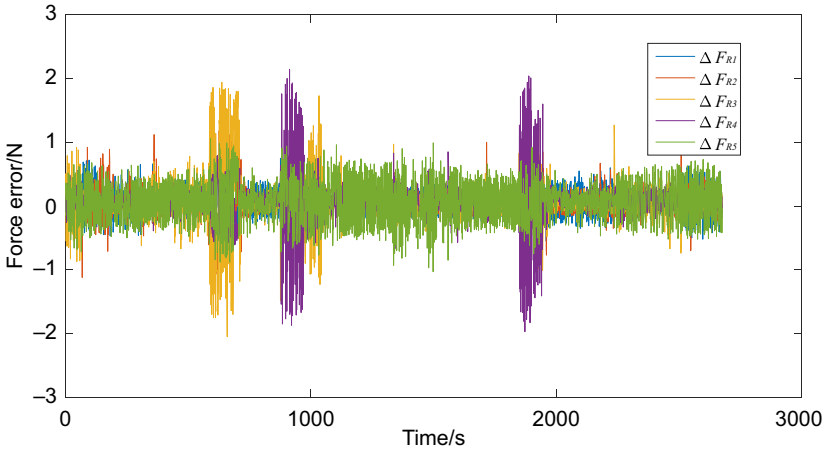

Fig. 14. Errors of suspension forces.

The manipulator operates according to a particular sequence, as shown in Fig. 13. The total time of the sequence is 2676 s. The maximum angle of the joint is ±30°; the angular velocity is ±0.1°/s. When the experiment starts, the manipulator executes the forward motion program. After a 30-s stop, the manipulator executes the backward motion program.

6.2. Experimental and theoretical joint torques

The force errors in five slings are measured by using tension sensor. As shown in Fig. 14, the deviations will not exceed 3N, which can be considered to achieve the constant force. By substituting the suspension forces, the force errors, the parameters of the manipulator, etc., in Eq. 10, the torques can be calculated .The experimental and theoretical torques of joints 1–6 are illustrated in Fig. 15.

The experiment results can verify the analyses in Section 5. The curves are rough due to the suspension tension errors and the flexible deformation. When joints 1, 3, 4 or 5 rotate, the torques of them have saltations. When joint 2 or 6 rotates, the torques of joints 2 and 6 have obvious changes, but the other joints are not sensitive to it. Except joints 2 and 6, the torque is larger when it is closer to the base. The errors of the back joints will accumulate to the front joints.

Compared with the collected data and calculated data, it shows that the theoretical torques are similar to the experimental ones, which can verify the accuracy of the theoretical derivation. When the actual space manipulator, which does not install the torque sensors in its joints, operates in the zero-g simulation system, the torques can be calculated by collecting the suspension forces. Furthermore, It can monitor whether the torque beyond the threshold guarantees the safety of the manipulator and the simulation system.

https://doi.org/10.1017/S0263574718001546 Published online by Cambridge University Press

Table III. Experimental and theoretical unloading ratios.

Joint label	**1**	**2**	**3**	**4**	**5**	**6**	**7**	**Total**
Calculated data	0.440	0.922	0.877	0.861	0.825	0.789	0.978	0.752
Collected data	0.438	0.926	0.853	0.872	0.814	0.790	0.977	0.749
Error	0.46%	−0.43%	2.8%	−1.3%	1.4%	−0.13%	0.10%	0.40%

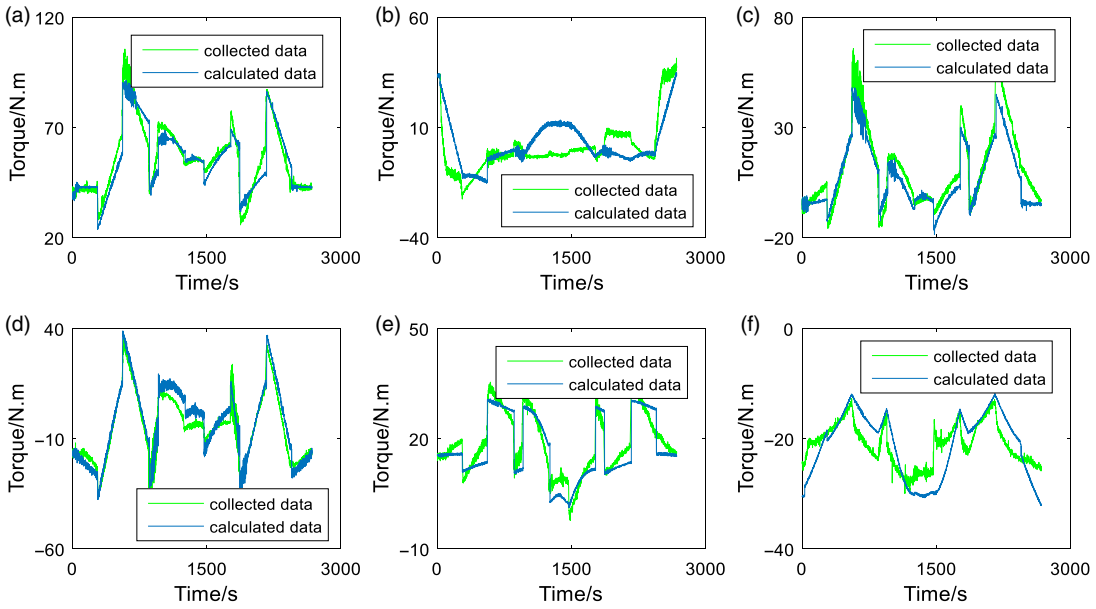

Fig. 15. Experimental and theoretical torques of joint. (a) Torque of joint 1; (b) torque of joint 2; (c) torque of joint 3; (d) torque of joint 4; (e) torque of joint 5; and (f) torque of joint 6.

6.3. Analysis and evaluation of unloading ratio

The experimental and theoretical unloading ratios of each joint and the total system are compared in Table III. Their deviation relative to the experimental values are less than 2%. The results verify that the derivation of the joint torques is correct and effective.

In this experiment, the total unloading ratio is 0.749, the single joint is no more than 0.438. It can be considered that this zero-g simulation system can simulate the zero-g environment in space to some extent. While, because of some unavoidable errors such as the frictions and the suspension forces, the deviations cannot be eliminated.

7. Conclusions

In this paper, a dynamic model of a seven-joints manipulator operated in a zero-g simulation system was established. The frictions, the errors of suspension forces and the flexible deformation of arms were considered as well. Inputting the suspension forces, parameters of the structure and mass of the manipulator and the joint angles, the torque of each joint can be calculated. The experiment was conducted as well. It verifies the safety of this simulation system and the accuracy of the dynamic model.

In addition, the unloading ratio was presented as the evaluation index of the zero-g simulation system. It can evaluate the level of similarity between the simulation system and the space environment. The more the unloading ratio closes to 1, the better the results of simulation will be. Meanwhile, the analysis and evaluation results of the unloading ratio were close, which can verify the accuracy of theoretical model as well.

In the future experiments involving the actual space manipulator which does not install the torque sensors, we can obtain the joint torques by substituting the collected data into the theoretical model. It can guarantee the safety of the experiments.

https://doi.org/10.1017/S0263574718001546 Published online by Cambridge University Press

Acknowledgments

This research was supported by the National Natural Science Foundation of China (No. 91648107) and the Beijing Natural Science Foundation-Haidian Original Innovation Joint Fund (No. L182041).

References

1. A. Flores-Abad, O. Ma, K. Pham and S. Ulrich, "A review of space robotics technologies for on-orbit servicing," *Prog. Aerosp. Sci.* **68**(8), 1–26 (2014).
2. A. Ellery, J. Kreisel and B. Sommer, "The case for robotic on-orbit servicing of spacecraft: Spacecraft reliability is a myth," *Acta Astronaut.* **63**(5), 632–648 (2008).
3. M. M. Alshibli, "Modeling and control of a free-flying space robot interacting with a target satellite," *Mech. Industrial Eng.*, 15–16 (2005).
4. Y. U. Dengyun, "Suggestion on development of Chinese space manipulator technology," *Spacecraft Eng.* **16**(4), 1–8 (2007).
5. H. Fujii, H. Yoneoka and K. Uchiyama, "Experiments on Cooperative Motion of a Space Robot," *Ieee/rsj International Conference on Intelligent Robots and Systems '93, IROS*, vol. 3 (1993) pp. 2155–2162.
6. Q. Yang and H. W. Liu, "Robot Modeling and Simulation Analysis of Micro-gravity Conditions," *4th International Conference on Computer, Mechatronics, Control and Electronic Engineering*, 985–990 (2015).
7. Y. Sato, A. Ejiri, Y. Iida and S. Kanda, "Micro-g Emulation System Using Constant-Tension Suspension for a Space Manipulator," *Proceedings of the 1991 IEEE International Conference on Robotics and Automation*, vol. 3 (1991) pp. 1893–1900.
8. L. I. Junshan, X. U. Min, S. Zhang and J. Chu, "Design of ground microgravity compensation experiment system based on the suspension spring," *Machinery Electronics*, vol. 8 (2014) pp. 34–37.
9. Z. Liu, "Gravity compensation for rocker-bogie rovers through single string tension," *J. Mech. Eng.* **49**(7), 113–124 (2013).
10. S. Tian, X. Tang and C. Xiang, "Equivalence analysis of mass and inertia for simulated space manipulator based on constant mass. *Machines* **5**(4), 31 (2017).
11. M. H. Korayem, A. Heidari and A. Nikoobin, "Maximum allowable dynamic load of exible mobile manipulators using finite element approach," *Int. J. Adv. Manuf. Tech.* **36**(5–6), 606–617 (2008).
12. X. Zhang, Y. Huang, X. Chen and W. Han, "Modeling of a space exible probecone docking system based on the kane method," *Chinese J. Aeron*, **27**(2), 248–258 (2014).
13. H. Liu and Y. Huang, "Robust adaptive output feedback tracking control for fiexible-joint robot manipulators based on singularly perturbed decoupling," *Robotica*, **36**(6), 822–838 (2018).
14. I. M. Da Fonseca, L. C. S. Goes, N. Seito, M. K. da Silva Duarte and E. J. de Oliveira, "Attitude dynamics and control of a spacecraft like a robotic manipulator when implementing on-orbit servicing," *Acta Astron.* vol. 137 (2016) pp. 490–497.
15. G. Morel, K. Iagnemma and S. Dubowsky, "The precise control of manipulators with high joint-friction using base force/torque sensing," *Automatica* **36**(7), 931–941 (2000).
16. H. B. Jr Brown and J. M Dolan, "A novel gravity compensation system for space robots," Nov. 11, 250 (1994).
17. J. Lpez-Martnez, D. Garca-Vallejo, A. Gimenez-Fernandez and J. L. Torres-Moreno, "A flexible multibody model of a safety robot arm for experimental validation and analysis of design parameters," *J. Comput. Nonlin. Dyn.* **9**(1), 1–10 (2014).
18. L. Simoni, M. Beschi, G. Legnani and A. Visioli, "Modelling the temperature in joint friction of industrial manipulators," *Robotica*, 1–22 (2017).
19. J. Arvo, "Fast random rotation matrices," *Graphics Gems III* (1992) pp. 117–120.
20. Q. Zheng, Q. Tang and L. Zhang, "Review of modelling and analysis methods of space manipulators," *Manned Spaceflight* **23**(1), 82–96 (2017).
21. T. W. B. Kibble and F. H. Berkshire, *Classical Mechanics* (5th ed.), (Imperial College Press, London, 2004) p. 236.